NANO LETTERS

xxxx
Vol. 0, No. 0
A−F

Controlled Multistep Purification of Single-Walled Carbon Nanotubes

Ya-Qiong Xu,[†,§] Haiqing Peng,[‡,§] Robert H. Hauge,[‡,§] and Richard E. Smalley*[,‡,§]

Department of Electrical & Computer Engineering, Department of Chemistry, and Carbon Nanotechnology Laboratory, Rice University, MS-100, 6100 Main Street, Houston, Texas 77005

Received October 15, 2004; Revised Manuscript Received December 1, 2004

ABSTRACT

A controlled and scalable multistep purification method has been developed to remove iron impurity and nonnanotube carbon materials from raw single-walled carbon nanotubes (SWNTs) produced in the HiPco (high-pressure CO) process. In this study, iron nanoparticles, coated by carbon, are exposed and oxidized by multiple step oxidation at increasing temperatures. To avoid catalytic oxidation by iron oxide of carbon nanotubes, the exposed and oxidized iron oxide is deactivated by reaction with $C_2H_2F_4$ or SF_6. The iron fluorides are removed by a Soxhlet extraction with a 6 M HCl solution. The purity and quality of each sample were determined by thermogravimetric analysis (TGA), Raman spectrometry, ultraviolet–visible-near-IR (UV–vis–near-IR) spectrometry, fluorescence spectrometry, and transmission electron microscope (TEM) spectroscopy. The purity and yield of SWNTs are improved due to reduced catalytic activity of the iron oxide. Greater iron oxide removal also resulted from oxidation at higher temperatures.

In recent years, single-walled carbon nanotubes (SWNTs) have been intensively studied because of their many potential applications. The high-pressure CO (HiPco) process, where $Fe(CO)_5$ is used as catalyst, is one of the most productive methods for SWNT production.[1−3] However, the iron and nonnanotube carbon impurities in the produced material need to be removed without damaging the SWNT. To remove catalyst (typically iron, cobalt, and nickel) and obtain high-purity SWNTs, many purification methods have been reported previously.[4−26] A common approach has been to use strong oxidation followed by an acid treatment. An oxidative treatment of raw SWNT material is effective in removing nonnanotube carbon and exposing the metal catalysts by removing carbon coating. However, nanotubes can be lost or damaged during the oxidation process. It is desirable that a scalable cleaning method only removes carbon impurities and metal catalysts without damaging nanotubes.

In this study, we report a scalable multistep purification method to remove metal catalysts and remove nonnanotube carbon from raw HiPco SWNTs. Our scalable multistep purification method includes two processes: oxidation and deactivation of metal oxides. In the oxidation process, metal catalysts coated by nonnanotube carbon are oxidized by O_2 and exposed in multiple steps with increasing temperature steps (150 °C through 350 °C). In the deactivation step, exposed metal oxides are deactivated by conversion to metal fluorides through reacting with $C_2H_2F_4$, SF_6, or other fluorine-containing gases to avoid the catalytic effect of iron oxide on SWNT oxidation. The proposed mechanism of purification is shown in Scheme 1.

Figure 1 shows the thermal gravimetry analyses of raw HiPco SWNTs in N_2/O_2, $N_2/O_2/C_2H_2F_4$, and $N_2/O_2/SF_6$ as function of time during heating. Weight gain during the initial heating is caused by the oxidation of iron particles. We found that all raw HiPco material is burned out at 325 °C in air within less than 5 min without fluorine-containing gases. It is well-known that purified SWNTs will not oxidize at temperatures lower than ∼350 °C,[12] so the catalytic effect of iron oxide on nanotube oxidation is obvious. However, when 5% $C_2H_2F_4$ or SF_6 gas was added into the N_2/O_2, the weight loss was less than 40% after heating at 350 °C for 6 h. This means that $C_2H_2F_4$ and SF_6 can efficiently deactivate the iron oxide and suppress the oxidation rate of SWNTs.

In our purification experiments, the samples (typically 10∼40 g) were placed in a 5 in.-diameter quartz reactor which was centered in a 6 in.-diameter horizontal quartz tube in a furnace. Nitrogen (1 L/min) was flowed both inside and outside of the reactor and maintained at atmospheric pressure. After purging the sample with 1 L/min N_2 at 150 °C, 200 mL/min O_2 and 50 mL/min SF_6 were turned on for 1 h. After this oxidation step, O_2 was turned off and the temperature was then ramped to 175 °C within half an hour while 50 mL/min SF_6 was maintained to deactivate the exposed metal catalysts. After this deactivation step, O_2 was turned on again

* Corresponding author: Tel: 713-348-4845. Fax: 713-348-5320. Email: smalley@rice.edu.
† Department of Electrical & Computer Engineering.
‡ Department of Chemistry.
§ Carbon Nanotechnology Laboratory.

10.1021/nl048300s CCC: $30.25
Published on Web 00/00/0000

Scheme 1. Chemical Reaction in the Oxidation and Deactivation Processes[a]

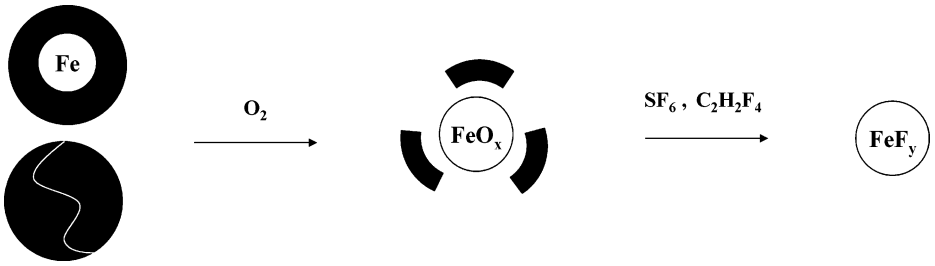

[a] The black color represents the carbon shell. The white curve on the black cycle represents a seam on the carbon shell. The white cycle is metal particle, metal oxide or metal fluoride. During oxidation the carbon shell reacts with the oxygen and produces carbon dioxide, and the metal is converted into metal oxide. During deactivation, the fluorine-containing gas converts the metal oxide into metal fluoride and deactivates the metal catalyst.

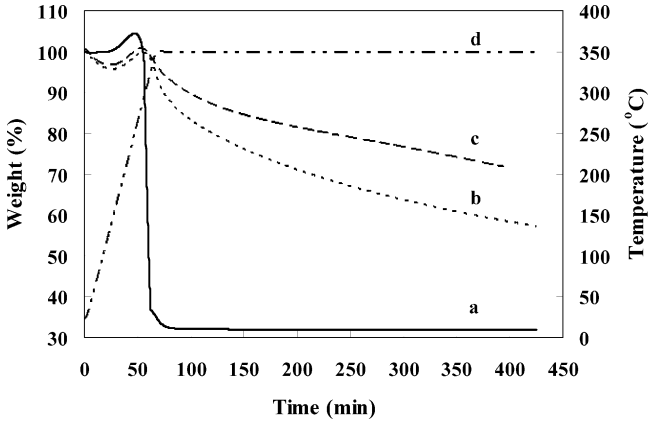

Figure 1. TGA of raw HiPco tubes heated in different gases. (a) 20% O_2, (b) 20% O_2 and 5% $C_2H_2F_4$, (c) 20% O_2 and 5% SF_6, (d) temperature.

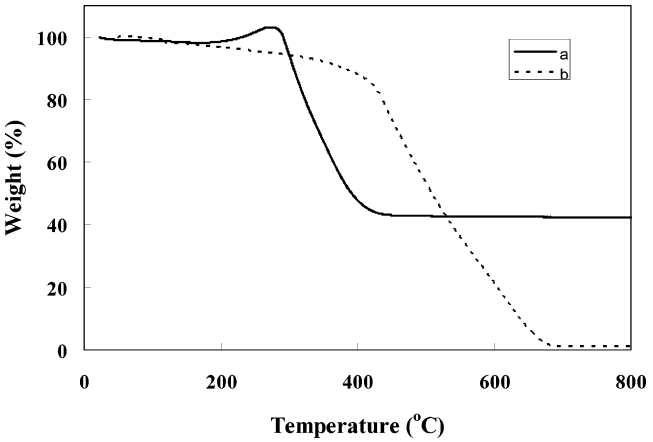

Figure 2. (a) TGA of raw and purified tubes heated in the dry air. (b) Raw material, samples purified with 20% O_2 and 1% SF_6.

for 1 h while the temperature was maintained at 175 °C. The oxidation/deactivation processes were repeated with a 25 °C increase up to 350 °C. The temperature and gas flow rate changes were controlled by a LABVIEW program. The finished sample was then cooled in N_2. Finally, the exposed metal was removed by 6 M HCl Soxhlet extraction for 12 h. The purified SWNT was extracted with hexane and dried in a vacuum at 50 °C for 24 h.

The purity and quality of each sample were documented by TGA, Raman, UV−vis−near-IR, and transmission electron microscope (TEM) spectroscopy. The purity of the cleaned sample is typically higher than 98 wt % with a carbon yield near 70%. TGA data was recorded with a TA Instruments Q500-TGA analyzer. In all experiments, samples (typically ∼10 mg) in an alumina pan were heated in dry air (100 mL/min) to 800 °C at a rate of 5 °C/min. Figure 2 shows the weight loss behavior of raw and purified SWNTs in dry air. This set of data demonstrates that the purified samples are stable in air at temperatures as high as ∼450 °C and their Fe contents are reduced from 30 wt % to approximately 1 wt %. TEM images were also obtained with a JEOL 2010 TEM at 100 kV. The samples were prepared by sonicating SWNTs in acetone and dropping the suspension onto lacey carbon grids. As shown in Figure 3, metal particles are identified as the dark particles. The metal particles are aggregated and associated with large fullerenes in the raw materials. In the purified sample shown in Figure 3b, metal particles and fullerenes are absent. Rough edges on the nanotubes are likely due to a small amount of remaining nonnanotube carbon and large fullerenes. In addition, the software from Smart Imaging Technologies was used to measure the size of metal particles in raw materials. The diameter distribution of metal particles is shown in Figure 3c. The average diameter was found to be ∼3 nm.

Raman, UV−vis−near-IR and fluorescence spectra show that there is little damage to the nanotube during the purification process. Raman spectra were collected with a Renishaw micro-Raman spectrometer equipped with a 780 nm laser and are shown in Figure 4. Typical SWNT Raman features are observed for the tangential modes and radial modes near 1591 and 200 cm^{-1}, respectively. The D-peak (1291 cm^{-1}) can be activated by disordering in the sidewall of the SWNT and identified with sidewall defects. We found that the ratio of the D-peak (1291 cm^{-1}) to G-peak (1591 cm^{-1}) decreases after purification. We also observed a change in relative intensity for various peaks of the breathing mode from raw material to purified samples, which suggests that the content of smaller diameter SWNTs has increased relative to the larger diameter ones. However, it is likely that this relative intensity change is due to a different coupling of the electronic resonance enhanced spectra to the Raman laser (782 nm) rather than to a relative change in tube diameter populations in the purified sample. In fact, electronic spectra such as UV−vis−near-IR spectra and fluorescence spectra,

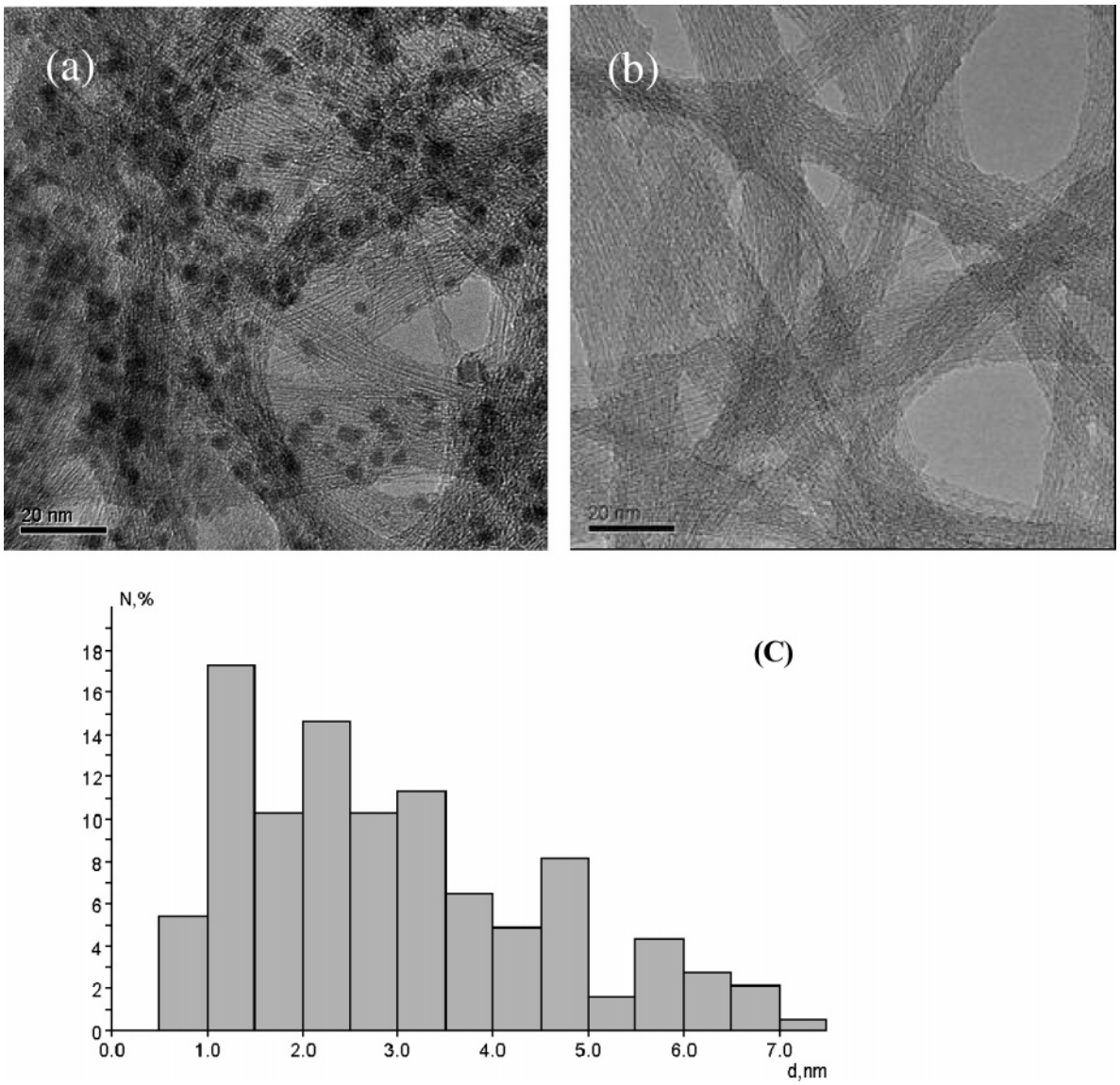

Figure 3. TEM images of (a) raw material and (b) purified sample, treated with 20% O_2 and 5% SF_6.

which we believe to be more reliable measures of tube diameter distribution, shown in Figure 5 and Figure 6 respectively, indicate that small diameter tubes are preferentially lost or functionalized in the purification process. UV−vis−near-IR spectra were obtained with a Shimadzu UV-3101 PC spectrometer. SWNT samples were dispersed in 1 wt % SDS surfactant, homogenized for 1 h, sonicated for 10 min in a cup-horn sonicator (Cole-Parmer CPX-600), and centrifuged for 4 h at 29000 rpm. The decant (the upper 75% to 80% of supernatant) was adjusted to pH=10 for UV−vis−near-IR experiments.[27] Figure 5 shows the UV−vis−near-IR spectra of SWNTs as raw material, 20% O_2 and 5% $C_2H_2F_4$ cleaned, 20% O_2 and 5% SF_6 cleaned, and 20% O_2 and 1% SF_6 cleaned samples. The spectra between 800 nm and 1300 nm wavelength show the first van Hove transition, E_{11}. From (b) to (d), the carbon yields decrease from 68% to 36%, as shown in Table 1, while the peaks corresponding to the smaller diameter tubes decrease as well, especially the peak near 1100 nm. These UV−vis−near-IR spectra indicate a preferential loss of smaller diameter tubes during the purification process. This indicates that the reactivity of the single-walled carbon nanotube is directly related to the pi-orbital mismatch caused by an increased curvature, which causes smaller diameter nanotubes to be more reactive. We performed fluorescence spectroscopic measurements with a J-Y Spex Fluorolog 3-211 equipped with an indium−gallium−arsenide near-infrared detector cooled by liquid nitrogen.[28] Emission intensity was measured as a function of emission wavelength (from 800 to 1570 nm), with excitation wavelength 669 nm, 1-nm steps and 3-nm spectral slit widths. Samples were prepared by the same method as those for UV spectra. Figure 6 shows the fluorescence spectra of SWNTs as raw material, sample cleaned with 20% O_2 and 5% $C_2H_2F_4$, sample cleaned with 20% O_2 and 5% SF_6, and sample cleaned with 20% O_2 and 1% SF_6. There are no shifts in frequency between the purified sample and the raw material, which indicates that little sidewall damage and defects were produced by the purification process. In addition, we noted that peaks near 952 nm decreased as the carbon yield decreased from 68% to 36%,

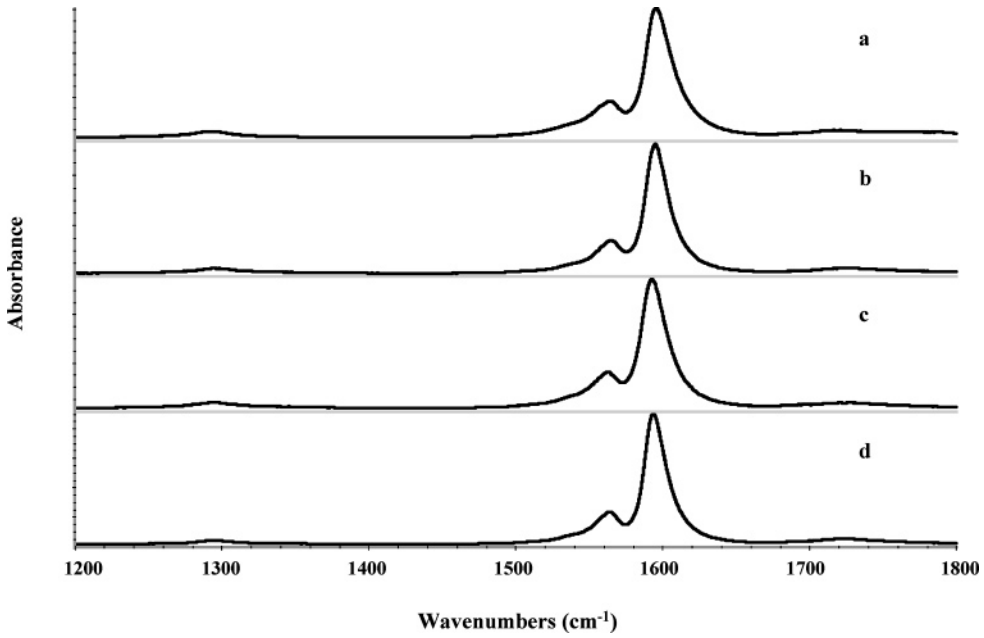

Figure 4. Raman spectrum of the raw and purified SWNTs: (a) raw material, (b) purified tubes with 20% O_2 and 5% $C_2H_2F_4$, (c) with 20% O_2 and 5% SF_6, (d) with 20% O_2 and 1% SF_6.

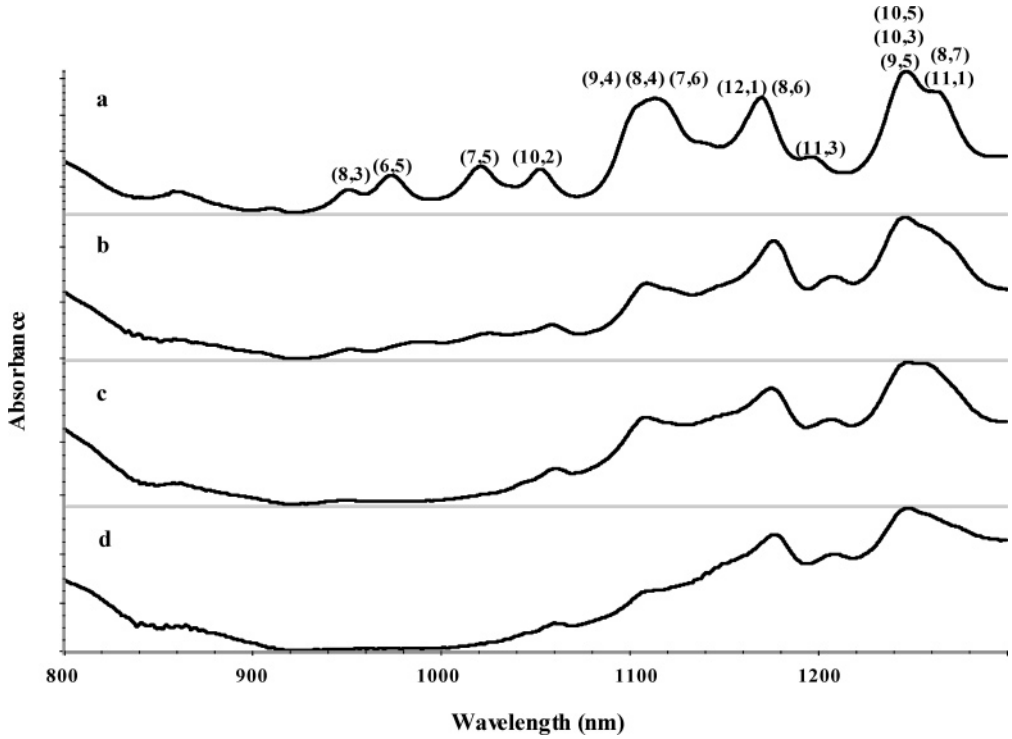

Figure 5. UV spectra of raw and purified SWNTs in 1% SDS at pH=10: (a) raw material, (b) purified tubes with 20% O_2 and 5% $C_2H_2F_4$, (c) with 20% O_2 and 5% SF_6, (d) with 20% O_2 and 1% SF_6.

as shown in Table 1. It indicates that (8, 3) nanotubes, which correspond to 952 nm, are more easily oxidized. Both Figure 5 and Figure 6 show that, during oxidation, smaller diameter nanotubes are readily oxidized as compared with larger diameter nanotubes.

In general, all purification methods of raw SWNT product expose the metal catalyst by oxidation. However, since metal oxides act as oxidizing catalysts, it is inevitable that some SWNTs will be lost. The yield of the purification procedure is highly dependent on controlling the oxidation process to prevent hot spot development and accelerated oxidation. In this cleaning process, control of catalytic oxidation is achieved by using a fluorine-containing gas to convert iron oxide into iron fluoride. In addition, during the oxidation and catalyst deactivation processes, we found that the progress of the reaction could be monitored by FT-IR spectroscopy of the effluent gases. This allows an in-situ investigation of gas-phase chemistry and enables the fol-

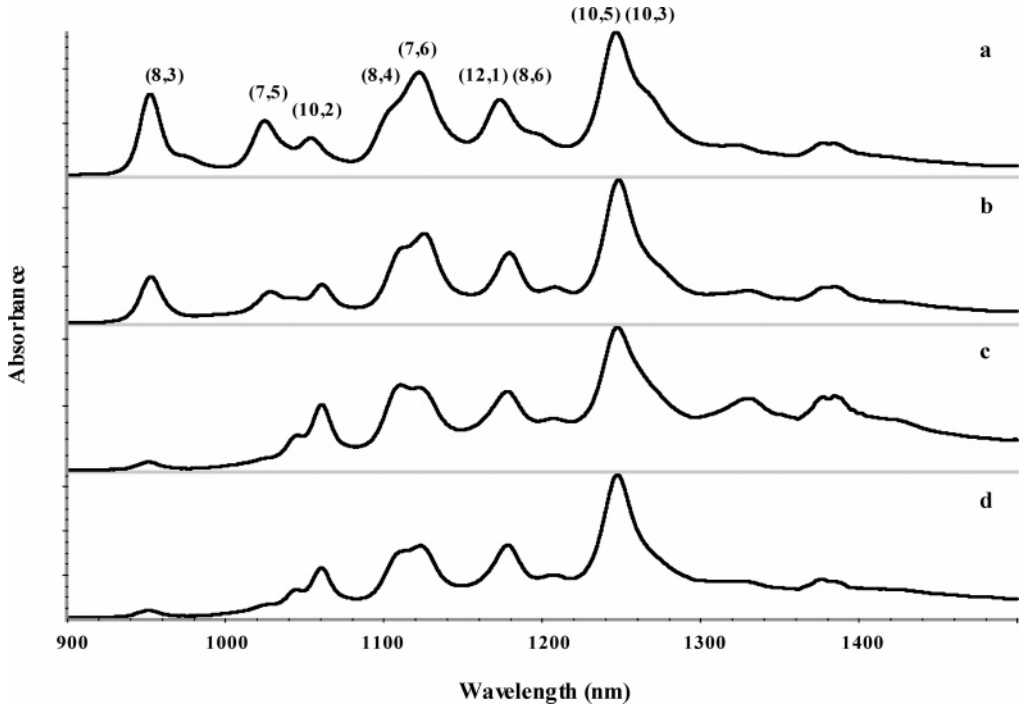

Figure 6. Fluorescence spectra of raw and purified SWNTs in 1% SDS at pH=10: (a) raw material, (b) purified tubes with 20% O_2 and 5% $C_2H_2F_4$, (c) with 20% O_2 and 5% SF_6, (d) with 20% O_2 and 1% SF_6.

Table 1. Carbon Yields of Different Purification Methods[a]

procedure	raw Fe wt %	purified Fe wt %	SWNT yield
multistep with 20% O_2 and 5%$C_2H_2F_4$	30%	1.5%	68%
multistep with 20% O_2 and 5% SF_6	30%	0.3∼1.3%	62%
multistep with 20% O_2 and 1% SF_6	30%	0.2∼0.5%	36%

[a] The SWNT Yield Is Defined as the Percentage of Purified SWNT to the Raw SWNT Excluding Metal.

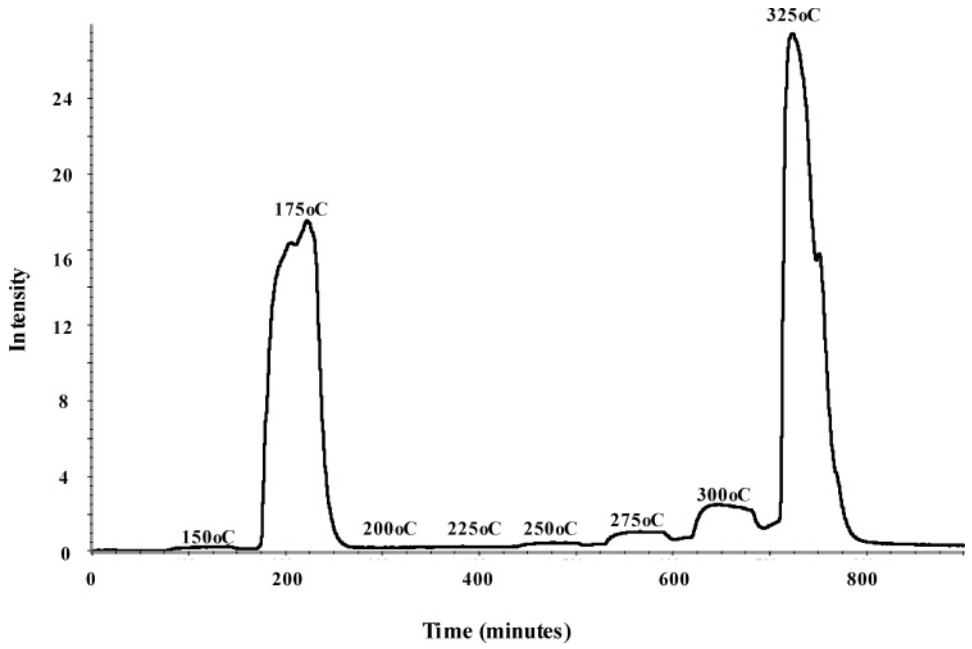

Figure 7. FI−IR spectra of CO_2 peak area between 3800 and 3500 cm^{-1}. In this experiment, we purify the raw material by 20% O_2 and 5% SF_6 and successively increase the temperature to 325 °C.

lowing of carbon etching without exposure of the sample to air. Because nonnanotube carbon is mostly large fullerenes for HiPco material, these impurities are more easily oxidized than are SWNTs. Therefore, at the beginning of the oxidation

process, most of the CO_2 and CO gas results from the oxidation of large fullerenes.

Figure 7 shows a series of FT-IR spectra of gas purification products as a function of time. From these spectra we follow carbon etching and monitor the oxidation reaction. This has allowed the optimization of the purification gas ratio and oxidation temperature. Table 1 shows carbon yields for different conditions. It is clear from these data that achieving the lowest iron contents results in the loss of small diameter nanotubes.

Our study provides a scalable multistep method for purifying raw SWNT samples. Characterization of purified material by using TEM, TGA, UV−vis−near-IR, fluorescence, and Raman spectroscopy clearly shows that the cleaned SWNTs have little sidewall damage. Iron content of approximately 1 wt % with approximately 70% SWNT yield can be achieved by in-situ fluoride deactivation of iron oxide catalyst particles.

Acknowledgment. The authors thank the Robert A. Welch Foundation, Advanced Technology Program of Texas, the National Aeronautics and Space Administration, Office of Naval Research and National Science Foundation for support of this research.

References

(1) Bronikowski, M. J.; Willis, P. A.; Colbert, D. T.; Smith, K. A.; Smalley, R. E. *J. Vac. Sci. Technol.* **2001**, *19*, 1800.
(2) Nikolaev, P.; Bronikowski, M. J.; Bradley, R. K.; Rohmund, F.; Colbert, D. T.; Smith, K. A.; Smalley, R. E. *Chem. Phys. Lett.* **1999**, *313*, 91.
(3) Thess, A.; Lee, R.; Nikolaev, P.; Dai, H. J.; Petit, P.; Robert, J.; Xu, C. H.; Lee, Y. H.; Kim, S. G.; Rinzler, A. G.; Colbert, D. T.; Scuseria, G. E.; Tomanek, D.; Fischer, J. E.; Smalley, R. E. *Science* **1996**, *273*.
(4) Hidefumi, H. *Mol. Cryst. Liq. Cryst. Sci. Technol., Sect. A* **1995**, *276*, 267.
(5) Yumura, M.; Uchida, K.; Niino, H.; Ohshima, S.; Kuriki, Y.; Yase, K.; Ikazaki, F. *Mater. Res. Soc. Symp. Proc. Novel Forms of Carbon II* **1994**, *349*, 231.
(6) Dillon, A.; Gennett, T.; Jones, K.; Alleman, J.; Parilla, P.; Heban, M. *Adv. Mater.* **1999**, *16*, 1354.
(7) Bandow, S.; Zhao, Z.; Ando, Y. *Appl. Phys. A* **1999**, *67*.
(8) Rinzler, A.; Liu, J.; Dai, H.; Nikolaev, P.; Huffman, C.; Rodriguez-Macias, F.; Boul, P.; Lu, A.; Heymann, D.; Colbert, D. T.; Lee, R.; Fischer, J.; Rao, A.; Eklund, P.; Smalley, R. E. *Appl. Phys. A* **1998**, *67*, 29.
(9) Dujardin, E.; Ebbesen, T.; Krishnan, A.; Treacy, M. *Adv. Mater.* **1998**, *10*, 611.
(10) Hiura, H.; Ebbesen, T.; Tanigaki, T. *Adv. Mater.* **1995**, *7*, 275.
(11) Chiang, I. W.; Brinson, B. E.; Smalley, R. E.; Margrave, J. L.; Hauge, R. H. *J. Phys. Chem. B* **2001**, *105*, 1157.
(12) Chiang, I. W.; Brinson, B. E.; Huang, A. Y.; Willis, P. A.; Bronikowski, M. J.; Margrave, J. L.; Smalley, R. E.; Hauge, R. H. *J. Phys. Chem. B* **2001**, *105*, 8297.
(13) Banerjee, S.; Wong, S. S. *J. Phys. Chem. B* **2002**, *106*, 12144.
(14) Borowiak-Palen, E.; Pichler, T.; Liu, X.; Knupfer, M.; Graff, A.; Jost, O.; Pompe, W.; Kalenczuk, R. J.; Fink, J. *Chem. Phys. Lett.* **2002**, *363*, 567.
(15) Farkas, E.; Anderson, M. E.; Chen, Z.; Rinzler, A. G. *Chem. Phys. Lett.* **2002**, *363*, 111.
(16) Georgakilas, V.; Voulgaris, D.; Vazquez, E.; Prato, M.; Guldi, D. M.; Kukovecz, A.; Kuzmany, H. *J. Am. Chem. Soc.* **2002**, *124*, 14318.
(17) Harutyunyan, A. R.; Pradhan, B. K.; Chang, J.; Chen, G.; Eklund, P. C. *J. Phys. Chem. B* **2002**, *106*, 8671.
(18) Hou, P.; Liu, C.; Tong, Y.; Xu, S.; Liu, M.; Cheng, H. *J. Mater. Res.* **2001**, *16*, 2526.
(19) Hu, H.; Zhao, B.; Itkis, M. E.; Haddon, R. C. *J. Phys. Chem. B* **2003**, *107*, 13838.
(20) Moon, J.; An, K. H.; Lee, Y. H.; Park, Y. S.; Bae, D. J.; Park, G. *J. Phys. Chem. B* **2001**, *105*, 5677.
(21) Niyogi, S.; Hu, H.; Hamon, M. A.; Bhowmik, P.; Zhao, B.; Rozenzhak, S. M.; Chen, J.; Itkis, M. E.; Meier, M. S.; Haddon, R. C. *J. Am. Chem. Soc.* **2001**, *123*, 733.
(22) Sen, R.; Rickard, S. M.; Itkis, M. E.; Haddon, R. C. *Chem. Mater.* **2003**, *15*, 4273.
(23) Smith, M. R.; Hedges, S. W.; LaCount, R.; Kern, D.; Shah, N.; Huffman, G. P.; Bockrath, B. *Carbon* **2003**, *41*, 1221.
(24) Thien-Nga, L.; Hernadi, K.; Ljubovic, E.; Garaj, S.; Forro, L. *Nano Lett.* **2002**, *2*, 1349.
(25) Zhao, B.; Hu, H.; Niyogi, S.; Itkis, M. E.; Hamon, M. A.; Bhowmik, P.; Meier, M. S.; Haddon, R. C. *J. Am. Chem. Soc.* **2001**, *123*, 11673.
(26) Zimmerman, J.; Bradley, R.; Huffman, C.; Hauge, R. H.; Margrave, J. L. *Chem. Mater.* **2000**, *12*, 1361.
(27) O'Connell, M. J.; Bachilo, S. M.; Huffman, C. B.; Moore, V. C.; Strano, M. S.; Haroz, E. H.; Rialon, K. L.; Boul, P. J.; Noon, W. H.; Kittrell, C.; Ma, J.; Hauge, R. H.; Weisman, R. B.; Smalley, R. E. *Science* **2002**, *297*, 593.
(28) Bachilo, S. M.; Strano, M. S.; Kittrell, C.; Hauge, R. H.; Smalley, R. E.; Weisman, R. B. *Science* **2002**, *298*, 2361.

NL048300S